Journal of King Saud University – Science 35 (2023) 102909

HOSTED BY

Contents lists available at ScienceDirect

Journal of King Saud University – Science

journal homepage: www.sciencedirect.com

Original article

Formulation, characterization and evaluation of gelatin-syringic acid/ zinc oxide nanocomposite for its effective anticancer, antioxidant and anti-inflammatory activities

M. Lavanya [a], Rajapandiyan Krishnamoorthy [b], Mohammad A. Alshuniaber [b], Salim Manoharadas [c], Chella Perumal Palanisamy [d], Vishnu Priya Veeraraghavan [e], Selvaraj Jayaraman [e], Ponnulakshmi Rajagopal [f,*], Ramakrishnan Padmini [a,*]

[a] Department of Biochemistry, Vels Institute Of Science, Technology, and Advanced Studies, Vels University, Chennai 600117, India
[b] Department of Food Science and Nutrition, College of Food and Agriculture Sciences, King Saud University, Riyadh 11451, Kingdom of Saudi Arabia
[c] Department of Botany and Microbiology, College of Science, King Saud University, P.O. BOX 2454, Riyadh, Saudi Arabia
[d] State Key Laboratory of Biobased Material and Green Papermaking, College of Food Science and Engineering, Qilu University of Technology, Shandong Academy of Science, Jinan 250353, China
[e] Centre of Molecular Medicine and Diagnostics (COMManD), Department of Bio-chemistry, Saveetha Dental College & Hospitals, Saveetha Institute of Medical & Technical Sciences, Saveetha University, Chennai 600077, India
[f] Department of Central Research Laboratory, Meenakshi Ammal Dental College and Hospital, Meenakshi Academy of Higher Education and Research (Deemed to be University), Chennai 600 095, India

ARTICLE INFO

Article history:
Received 13 June 2023
Revised 13 September 2023
Accepted 16 September 2023
Available online 22 September 2023

Keywords:
Zinc oxide nanoparticle
Syringic acid
Gelatin
Hep G2 cell line
Antioxidant
Anti-inflammatory

ABSTRACT

Background: Hepatocellular carcinoma (HCC) is the most typical form of liver cancer. Apart from modern therapies, various natural chemical constituents have been tested for the treatment of HCC. However, the usage of the latter has declined due to their low bioavailability and stability.
Objectives: Considering the above drawback's, in this study, we describe a gelatin-syringic acid/ zinc oxide (ZnO) nanocomposite for liver cancer treatment, which showed antioxidant, anti-inflammatory and anticancer activities.
Methods: The hydrothermal method was used to synthesize ZnO nanoparticle and it was encapsulated with gelatin-syringic acid by coacervation technique. The nanocomposites were characterized by UV spec, FTIR, SEM, XRD, EDX, and DLS. The drug release profile of nanocomposite was studied by dialysis bag method, which exhibits a sustained drug release.
Results: The antioxidant ability of nano-composite was studied by performing an ABTS and DPPH assay and the IC50 was recorded as 76.5 and 47.63 μg/mL, respectively. The anti-inflammatory potential was studied by assessing the ability of nanocomposite on denaturation of protein and the results exhibited a dose-dependent inhibition. The acute toxicity of nanocomposite tested on zebrafish liver and heart showed that it is non-toxic. Moreover, the nanocomposite inhibits the Hep G2 cell viability with an increasing concentration and it increases oxidative stress caused by the mitochondrial damage, which leads to cell death.
Conclusion: Based on the findings of the present study, gelatin-syringic acid/ZnO nanocomposite has been shown to possess antioxidant, and anti-inflammatory properties, and thus can be used against HCC.

* Corresponding authors.
E-mail addresses: lavanya.phd@velsuniv.ac.in (M. Lavanya), moorthy@ksu.edu.sa (R. Krishnamoorthy), malshuniaber@ksu.edu.sa (M.A. Alshuniaber), smanoharadas@ksu.edu.sa (S. Manoharadas), chella.p@chula.ac.th, kalaiselvik.sdc@saveetha.com (C. Perumal Palanisamy), vishnupriya@saveetha.com, swethap.sdc@saveetha.com (V. Priya Veeraraghavan), selvarajj.sdc@saveetha.com (S. Jayaraman), drponnulakshmi.researchscientist@madch.edu.in (P. Rajagopal), padmini.sls@velsuniv.ac.in (R. Padmini).
Peer review under responsibility of King Saud University.

Production and hosting by Elsevier

https://doi.org/10.1016/j.jksus.2023.102909
1018-3647/

1. Introduction

Since ancient times, humans have been utilizing plant-based products in treating many ailments. This traditional knowledge about natural products has been practiced for many generations in Ayurveda, Siddha, Unani, Chinese, and other traditional systems of medicine. Natural products are also used in modern medicine not only for disease treatment and but also in health maintenance (Watkins et al., 2015). As a result, natural materials are regarded as a critical repository for the development of potential novel drugs. Today, a vast majority of drug candidates are natural products or structural analogs of natural products. Though numerous natural compounds with therapeutic potential have been identified, their use as therapeutic agents is often limited because of their relatively low bioavailability, high metabolism, minimal absorption, and quick systemic elimination.

It has been proven that nanotechnology can control drug release to enhance the therapeutic benefits and regulate particles to target particular biological sites. In this milieu, nanoformulation of natural compounds or extracts offers several advantages, including resistance to degradation, enhanced solubility, and bioavailability (Mahesh et al., 2021). According to recent studies, nanoparticles can greatly enhance the bioavailability of natural compounds both in vitro and in vivo. After being incorporated into nanocarriers, plant secondary metabolites such as flavonoids, tannins, and terpenoids demonstrated a better therapeutic effect than their native form.

Studies have shown that the formulated nano curcumin by nanoemulsion technique exhibited a slow release of curcumin from nanoparticles, which hikes the curcumin bioavailability (Mohanty et al., 2012). The curcumin nanoparticle has been efficient against human laryngeal cancer. Hesperidin extracted from orange peels was nano-formulated by encapsulation and showed its impact on cytotoxicity and exhibits potential antioxidant property against three cancerous cell line [HCT-116, HepG-2, and MCF-7] (Habiba et al., 2021). Polymer encapsulated luteolin nanoparticles were studied in [Tu212] and [H292] cell lines and the nanoparticle formulations were found to be much more effective than luteolin alone because the tumor receptor binds with the target ligand on the nanoparticle surface and shows suppressed tumor activity (Majumdar et al., 2014).

Syringic acid, a phenolic phytochemical compound, is present in foods like acai palm, honey, red wine, olives, grapes, walnuts, dates, pumpkin, spices, and sugar apples. It is one such type of secondary metabolite, which has varied pharmacological effects. However, it is eliminated from the systemic circulation due to its low bioavailability. Syringic acid is adimethoxybenzene with a molecular weight of 198.17 g/mol, and its molecular formula is $C_9H_{10}O_5$. It possesses anti-oxidant, anti-cancer, anti-inflammatory, and antiendotoxic activity (Srinivasulu et al., 2018). In spite of its various therapeutic effects, its use in biomedical fields gets declined due to its poor solubility and bioavailability. To improve the solubility and bioavailability, the syringic acid can be encapsulated with a biopolymer (or) nanoparticle.

Recently, gelatin biopolymer is widely used by many researchers in sight of its applications such as the controlled release of drugs, and their capability to deliver drugs in optimal doses at targeted sites (Chanchal et al., 2012). Earlier research has shown that the gelatin-coated zinc oxide (ZnO) nanoparticle has anti-biofilm, antibacterial, and anti-angiogenicactivity. ZnO nanoparticles have wider applications than other metal oxide nanoparticles because of their excellent biocompatibility, affordability, low toxicity, and environmental friendliness (Mishra et al., 2017). Hassan HFH et al. (2017) studied the effect of zincoxide nanoparticle against Hep G2, PC3, and A549 cancer cell lines and on hepatocellular carcinoma. The study revealed that the ZnO nanoparticle decreased the level of biochemical markers, and increased the release of caspase 3, in ZnO treated groups, which lead to cancer cell death. Recently Khafaga et al. (2022) showed the anticancer effect of ZnO nanocomposite synthesized from Fusarium oxysporum on DEN induced HCC. Another study exhibited the apoptotic effect of ZnO nanoparticle against HCC, colorectal cancer, and breast cancer cell line. ZnO nanoparticles prepared with biopolymer exhibit a well-designed mode for drug release at the target site.

The present study describes the synthesis of gelatin-syringic acid/ZnO nanocomposite, its characteristics, syringic acid drug release from nanocomposite, antioxidant and anti-inflammatory properties, acute toxicity on zebrafish liver and heart, and invitro anticancer activity on Hep G2 cells.

2. Materials and methods

2.1. Materials

Sodium hydroxide [NaOH], Zinc acetate dehydrate[$(CH_3COO)_2Zn^*2H_2O$], gelatin, Syringic acid were purchased from Sigma Aldrich, St. Louis, Missouri, United States. Wild-type zebrafish strains (Daniorerio) were obtained from local fish aquarium. Hep G2 cell lines were procured from National Centre for Cell Science (NCCS), Pune, and Maharashtra.

2.2. Ethical approval

The approval from the Institutional Animal Ethics Committee (IAEC) was obtained for the acute toxicity study. The ICH harmonisation criteria for the housing and management of zebrafishwere followed throughout the study. The treatment of zebra fish was adhered to OECD guidelines (IAEC study No: 230/Go052021/IAEC).

2.3. Synthesis of zinc oxide nanoparticles

Zinc acetate and methanol were used as precursors in the hydrothermal technique to generate ZnO nanoparticles. Under stirring, a 0.1 M zinc acetate solution was made in 50 ml of methanol. Under constant stirring, 25 ml of a 0.2 M sodium hydroxide (NaOH) solution was added to this solution. The solution was then placed into a hot air oven for 3 h at 100 °C. After then, it was allowed to naturally cool to room temperature. The final white solid product of the reaction was filtered, washed with methanol, and then allowed to air dry in an incubator for a whole night at 60 °C.

2.4. Preparation of gelatin-syringic acid-zincoxide nanocomposite

The Coacervation technique was used to encapsulate gelatin-syringic acid. Gelatin and syringic acid of 0.5 g each were dissolved in 50 ml of sterile water and continuously stirred for 2 h. Simultaneously 15 g of prepared ZnO nanoparticles were dissolved in 50 ml of sterile water and subjected to stirring. The final step is the creation of a nanocomposite, which was accomplished by adding drop wise the gelatin-syringic acid solution to the ZnO nanoparticle solution under continuous stirring. Now the nanocomposite solution were allowed to stir for 2–3 h. Then the solution is filtered using Wattmann filter paper, and the nanocomposite residue is allowed to dry in an incubator at 60 °C for overnight and the prepared nanocomposite were stored for further analysis.

2.5. Characterization of synthesized nanocomposite

Shimadzu UV-1800, a UV–Visible spectrophotometer with a wavelength range of 200–650 nm, was used to examine the optical properties of the nanocomposite. By employing the Seifert 3000p with Cu-K radiation and two scanning ranges of 10–80($2\theta^0$), X-Ray Diffraction (XRD) was used to examine the crystallographic structure of a nanocomposite. Utilising the Bruker series for Fourier-transform infrared spectroscopy (FTIR). The functional groups included in the synthesized nanocomposite were examined using Fourier transform infrared spectroscopy over a broad spectral range of 4000–400 cm^{-1}. The surface morphology of the produced nanocomposite was examined using scanning electron microscopy (SEM), on a JEOL 2100, and its elemental concentration was quantified using Energy-dispersive X-ray spectroscopy (EDS). The dynamic light scattering (DLS) technique was used to calculate the size of the particles.

2.6. Drug release profile

The drug release profile nanocomposites were analyzed by dialysis bag method (Kalidas, s et al., 2022). Gelatin-syringic acid-zinc oxide nanocomposite release profiles were assessed in vitro in phosphate buffer solution (PBS) at pH 7.4. In 3 ml of PBS, 30 mg of the nanocomposite was suspended. To imitate the state in the body, the tubes were put in a water bath shaker at 37 °C with a swirling rate of 90 rpm. The tube was taken at certain intervals (0, 60, 90, 120, 150, 180, 210, 240, and 270 min.) and its absorbance was instantly measured using UV–Vis Spectroscopy at lambda max of 280 nm. The equation derived from the standard curve was used to calculate the amount of drug released.

2.7. Antioxidant assay

2.7.1. 2, 2′-azino-bis (3-ethylbenzothiazoline-6-sulfonic acid) assay

The stock solution of potassium persulfate (2.4 mM) and ABTS salt (7 mM) prepared in equal amounts were kept in dark for 16 hrs at 25 °C, and methanol was added in a small amount for complete dissolution. 1 ml of stock solution of different nanocomposite concentrations, ranging from 20 to 100 μg was added and the absorbance was measured at 734 nm to determine the number of free radicals. The experiment was repeated thrice for concordancy. Using the formula, the percentage inhibition was obtained.

$$\%\,\text{Inhibition} = 100(\text{control} - \text{test})/\,\text{Control}$$

2.7.2. 2, 2-diphenyl-1-picrylhydrazyl assay

To the 4% DPPH, the different concentration ranging 20–100 μg of synthesized nanocomposite were added and then kept at incubation for 30 min at room temperature. During the incubation period, the dark purple DPPH solution changes to a pale yellow color. At 517 nm, the absorbance was measured. The methanol mixed DPPH served as a blank and ascorbic acid was served as a control. The formula was used to determine the percentage inhibition.

$$\%\,\text{Inhibition} = 100(\text{control} - \text{test})/\,\text{Control}$$

2.8. Anti-inflammatory activity

2.8.1. Inhibition of albumin denaturation

The protein denaturation technique helps in identifying the anti-inflammatory activity. 1 ml of 1% albumin solution dissolved in 0.1 M PBS and pH 6.4, followed by the addition of test solution (1 ml) containing various concentration of nanocomposites (20–100 μg) make up the reaction mixture and heated to 60 °C for 10 min to cause the denaturation. The absorbance was measured at 660 nm after cooling. After cooling, the absorbances were evaluated at 660 nm. Sodium diclofenac was used as the positive control. Using the formula, the percentage inhibition was calculated.

$$\%\,\text{Inhibition} = 100(\text{control} - \text{test})/\,\text{Control}$$

2.9. Toxicology study

Generally, the toxicology study referred to as the "science of safety," is designed to study the toxic effect of a drug by identifying its impact on organ structure and function. The small size, inexpensive, rapid development, and accessible breeding house in a standard aquarium are the benefits of using zebrafish as an animal model than most accepted mice models. In this study, the acute toxicity, which includes the LD_{50}, organ morphology and cytology, swim velocity, survival rate, and novel dive tank test of zebra fish were analyzed for testing the toxic effect of the synthesized gelatin-syringic acid-zinc oxide nanocomposite.

2.9.1. Zebrafish husbandry

The zebrafish strains (Danio rerio) were used for the present cytotoxicity study. Before the experiment induction, all fishes were adjusted to the constant lab environment for at least one week in stock aquaria. The fish were fed with tetra bits pellets daily until the beginning of the experiment. Healthy adult males with no signs of infection, equivalent body size, and age were scrutinized and used for the experiment analysis. A light–dark cycle of 14:10 h with a water temperature of 27 +/- 1 °C and pH between 6.8 and 7 were adhered throughout the study. Once every 7 days, the washout process was carried out to keep the fish in a clean environment and to eliminate the risk of infection.

2.9.2. Feed preparation

The synthesized nanocomposite was measured for the known dilution volume and extruded to pellets of standard size weighing 4 mg per pellet. Throughout the study period, the pellets were fed to the fish twice a day. The first feed with compound feed and the second with the commercial feed.

2.9.3. Lethal dose (LD_{50}) study

During the course of the study, the fishes were treated with a logarithmic dose of the nanocomposite at 100 μg and 1000 μg for 48 h and the lethal events were observed in order to determine the LD_{50}. Since the nano composite was less toxic, a limit dose was performed with logarithmic doses of 1 ng, 10 ng, 100 ng, 10 μg, and 100 μg, and monitored for any adverse effects.

2.9.4. Acute toxicity study

The fish groups with 1 ng, 10 ng, and 100 ng of formulated nanocomposite loaded pellet were tested for acute toxicity study and the morphological and pathological changes were observed for 14 days. A control group was used parallel to the dosed group for dissection and investigation of vital organs such as the heart and liver. After the experimental period, the zebrafish from the respective group were euthanized by rapid cooling at 24 °C using ice chips and were subjected to dissection and the heart and liver tissue were observed for anatomical and cytological changes.

2.9.5. Novel dive tank test

For the dive tank test, a rectangle tank was filled with 20L of fish housing water to test the diving capacity of fish. The water level in the tank was divided horizontally into two halves indicating the active top zone and the inactive bottom spot. The fish were transferred to the novel tanks using hand-nets and immediately noted the observations for consecutive 3 min. Treated and control groups

were assayed alternately in identical tanks and pointed out for the number of seconds spent at the bottom and top zones.

2.9.6. Swim velocity

The study was intended to carry out the motor activity of the treated vs. control group in a rectangular tank. The assays were performed in a light cycle to eliminate the circadian-induced bias. The fish were introduced to the study tank and allowed to acclimate for 3 min; monitored the swimming velocity (mm/s) of the fish for 10 min, and counted the survival rate of the fish daily to understand the mortality curve over therapeutic intervention.

2.10. Invitro study on Hep G2 cell line

2.10.1. Cell line and culture medium

From National Centre for Cell Sciences (NCCS), located in Pune, India, the epithelial cell lines for human liver cancer (Hep G2) were purchased. A Dulbecco's modified eagle medium (DMEM) containing 10% (v/v) heat-inactivated foetal bovine serum (FBS), 100 g/mL streptomycin, and 100 U/mL penicillin was used to culture the cells. They were grown in an incubator (95% humidity) with 5% CO2 at 37 °C.

2.10.2. Cytotoxicity activity of gelatin-syringic acid/zno nanocomposite

By using the MTT (3-(4, 5-dimethylthiazol-2-yl)-2, 5-diphenyltetrazolium bromide assay), the cytotoxic effect of synthesized nanocomposite was evaluated against the HepG2 cell line. The cells were grown in 96-well microplates at a density of 1×10^6 cells per well and then cultured at 37 °C for 48 h in a 5% CO_2 incubator to reach 70–80% viability. The media was then replaced, and the cells were exposed to synthesized nanocomposite at different concentrations (20, 40, 60, 80, and 100 μg/ml) for 24 h. After 24 h, a digital inverted microscope (20 X magnification) analyzed morphological alterations in treated and non-treated cells. After washing the cells with phosphate-buffer saline (PBS, pH-7.4), 20 μl of the (MTT) solution (5 mg/mL in PBS) was injected into each of the well. After that, the plates were left at 37 °C in the shade for two hours. The absorbance was determined spectrophotometrically at 570 nm after the formazan crystals had been dissolved in 100 μl of DMSO. The percentage of cell viability was estimated using the following formula.

$$\text{Cell viability}\,(\%) = (\text{sample/control})\,\text{X}\,100$$

2.10.3. Apoptotic detection by AO/PI dual staining

In a 6-well plate, 1×10^5 Hep G2 cells per well were used to culture the cells, and they were exposed to synthesized nanocomposite at its IC50 concentration for 24 h. Hep G2 cells left untreated served as the control. After being rinsed with PBS, the treated cells were stained for 5 min with 20 μl of an AO/PI staining solution (100 g/ml AO&PI). Due to membrane stability impairment, AO stain is absorbed by live and dormant cells and emits green fluorescence, PIstain, in contrast only penetrates non-viable cells and produces red fluorescence. Fluorescence microscopes (40 × magnifications) were used to examine the stained cells.

2.10.4. Reactive oxygen species (ROS)

Intercellular ROSformation in synthesized nanocomposite exposed Hep G2 cells were assessed by oxidizingcell-permeable Dichloro-dihydro-fluorescein diacetate (DCFH-DA) into fluorescent 2,7dichlorofluorescein (DCF). Hep G2 cells (1×10^5 cells per well) were treated with nanocomposite at IC_{50} concentration, and the cells were then incubated for 24 h. 1 μl of DCFH-DA (1 mg/ml) were used to stained the treated cells and left in the dark for 20 min. The developments of DCF inside the cell were observed by fluorescence microscope.

2.10.5. Mitochondrial membrane potential (MMP)

The MMP is observed using the Rhodamine 123 stain, and cationic fluorescent dye. Hep G2 cells, were exposed to nanocomposite at IC_{50} concentration, and rinsed with Phosphate buffer saline. 50 μl of Rhodamine 123 (10 μg/ml) were used for staining, and then the cells were allowed to dry. The membrane permeability and structural changes were observed using a fluorescent microscope at 40-x magnification.

2.10.6. Statistical analysis

The MATLAB and SPSS software were used for calibrating the statistical values. Each study was carried out in triple, and the results were shown as mean ± standard error of mean.

3. Results

3.1. Ultraviolet visible spectroscopy

Fig. 1a represents the optical property of synthesized nanocomposite measured at a wavelength of 200–650 nm. The excitonic absorption peak observed at 280 nm defines nanomaterials; optical properties and presence with a band gap energy of 4.43 eV, calculated from the equation E = hc/λ..

3.2. X-ray diffraction study

In this study, thirty-eight XRD peaks are acquired for the synthesized nanocomposite is shown in Fig. 1b. Furthermore, the five prominent peaks with corresponding miller indices 32.509 (100), 33.200(002), 34.56 (101), 40.401 (102), and 59.281(110) indicate the presence of crystalline zinc oxide nanoparticles.

3.3. Fourier transform infrared spectroscopy analysis

The functional groups of synthesized nanocomposite analyzed using FTIR were shown Fig. 1c. The peaks around 3779–3232 cm^{-1} correspond to alcohols, the strong narrow peak at 1108 cm^{-1} corresponds to the C-O stretch, and the peaks around 1594–1616 cm^{-1} represent the N–H bend. A peak at 533 cm^{-1} represents the ZnO nanoparticle. Comparing the syringic acid and synthesized nanocomposite FTIR spectra shows the peak at 420 cm^{-1}, indicates the presence of syringic acid in the nanoformulation.

3.4. Scanning electron microscopy

SEM analysis was used to examine the morphology of a synthesized nanocomposite. The flaky structure of a synthesized nanocomposite was seen, particle size rise of about 1.11 nm was shown in Fig. 2a.

3.5. Energy dispersive x-ray spectroscopy analysis

Energy Dispersive X-ray Analysis was used to identify the chemical compositions of the nanocomposite. Fig. 2b and Table 1a depict the EDS and percentage analysis of elements present in the synthesized nanocomposite. The peaks demonstrate the presence of various elements, but the extreme elevation was

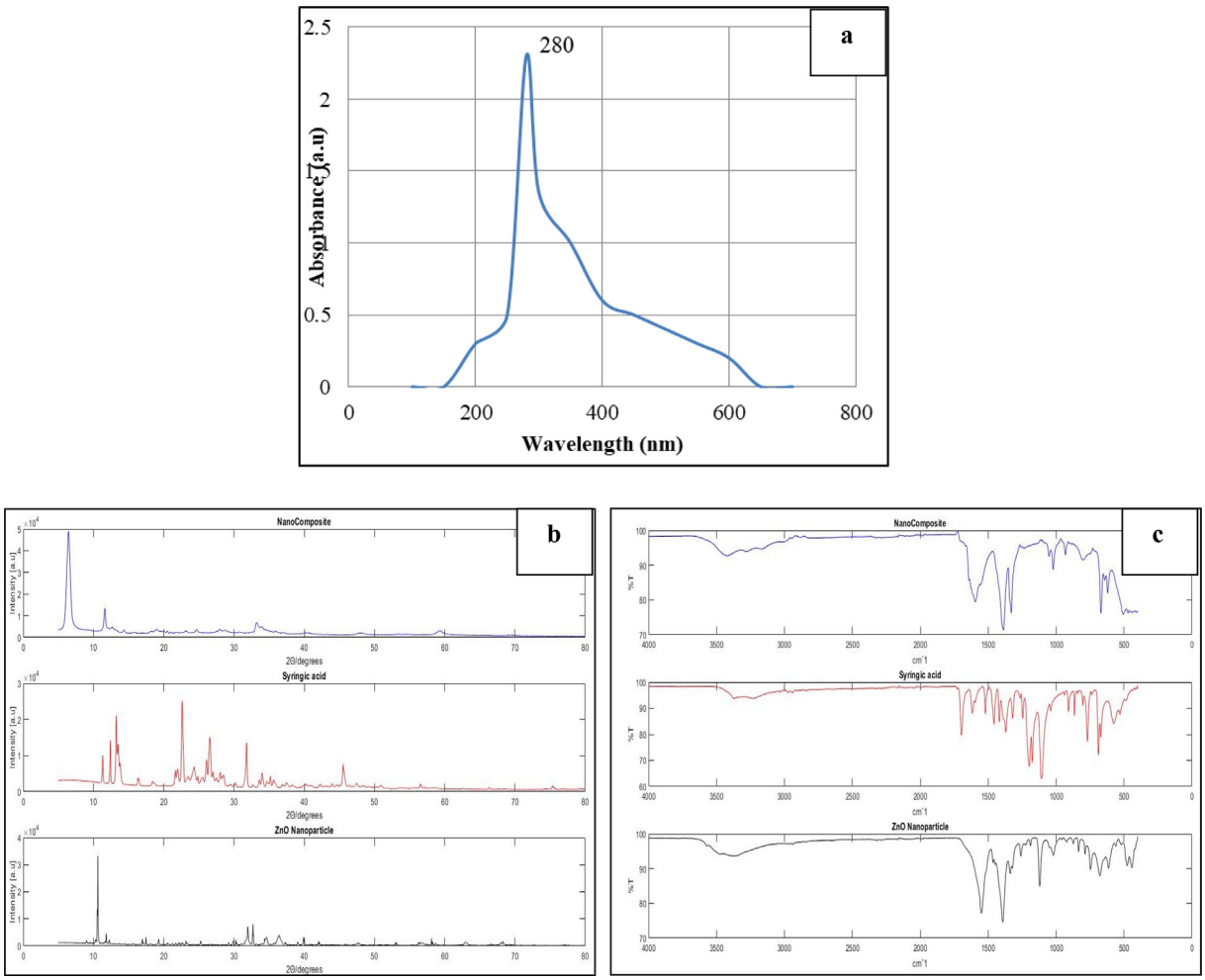

Fig. 1. A-c: 1a- uv– Visible spectral image of gelatin-syringic acid-zincoxide nanocomposite. 1b-Comparative X-ray diffraction of the nanocomposite, Syringic acid, and ZnO nanoparticle. 1c-FTIR Spectral image of nanocomposite,Syringic acid, and ZnO nanoparticle.

shown for zinc and oxygen, with yields of approximately 45.28% and 30.83%, respectively, the graph strongly supports the formation of zinc oxide nanoparticles in the synthesized nanocomposite.

3.6. Dynamic light scattering

The size dispersal profiles of the synthesized nanocomposite were examined by dynamic light scattering (DLS). The size dispersal of nanocomposite was shown in Fig. 2c. The poly dispersive index (PDI) is 0.4, which indicates the synthesized nano compound was monodisperse. The nanocomposite consists of molecules with the same chain length, and the PDI 0.4 is the excellent agreement with the size of the nano compound, as per earlier studies.

3.7. Drug release study

As a consequence of the experiments, it was found that syringic acid was rapidly released in phosphate buffer solution, with a cumulative release rate of almost 90% in 120 min. The gelatin, syringic acid, and zinc oxide nanocomposite exhibited a sustained-release action and were rapidly released, with a 60% cumulative release over the first 120 min and a following steady and gradual release. Fig. 2d shows the nanocomposite showed an evident sustained-release impact in vitro when compared to syringic acid.

3.8. Antioxidant activity

3.8.1. 2, 2′-azino-bis (3-ethylbenzothiazoline-6-sulfonic acid) (ABTS) assay

The radical scavenging activity of the synthesized nanocomposite was determined using the ABTS assay. The antioxidant capacity of a synthesized nanocomposite is shown in Table 1b. The radical scavenging activities such as 20.23 ± 1.24, 27.23 ± 1.21, 37.43 ± 1.38, 55.21 ± 1.21, 65.17 ± 1.18 μg/ml respectively at different concentrations (20–100 μg/ml) was observed and IC_{50} was observed to be 76.5 μg/ml. Similarly, the radical scavenging activities of ascorbic acid were performed and the results were between 25.46 ± 1.32 to 78.62 ± 5.55 μg/ml with increasing concentrations. The standard drug IC_{50} value was observed to be 68.6 μg/ml. Therefore, the nanocomposite showed the significant ABTS scavenging activity.

3.8.2. 2,2-diphenylpicrylhydrazyl assay

The radical scavenging activity of synthesized nanocomposite was analyzed by DPPH assay. The antioxidant capacity of a synthesized nanocomposite is shown in Table 2a. The radical scavenging activities such as 21.97 ± 1.29, 46.17 ± 1.18, 60.17 ± 1.18, 70.33 ± 1.22, 78.12 ± 1.12 μg/ml respectively at different concentrations (20–100 μg/ml) was observed and IC_{50} was observed to be 47.63 μg/ml. Similarly, the radical scavenging activities of ascorbic

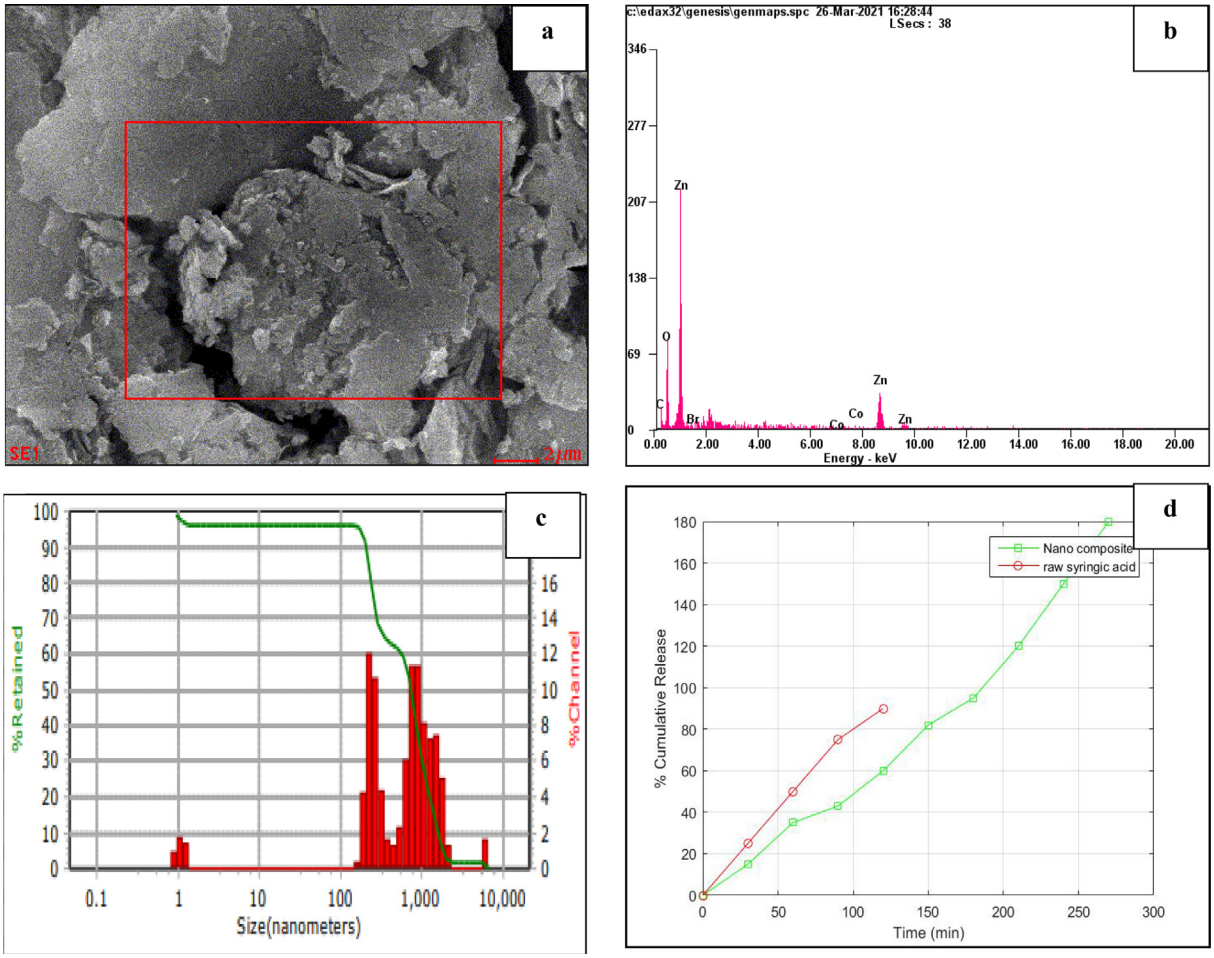

Fig. 2. A-d: 2a-sem micrograph illustrates the nanocomposite. 2b-eds reveals the elemental analysis of nanocomposite. 2c-The DLS graph displays the size distribution and average particle size of the nanoparticles. 2d-Drug release profile of nanocomposite and syringic acid were compared, in which the 90% of syringic acid were released at 120 min, whereas only 60% of drug from nanocomposite were released at 120 min. Thus, the nanocomposite shows the sustained and slow release than raw syringic acid.

Table 1a
Elemental composition of ZnO nanoparticle.

Element	Wt %	At %
Zinc	45.28%	15.36%
Oxygen	30.83%	42.74%

acid were performed and the results were between 27.55 ± 1.35 to 83.56 ± 4.46 µg/ml with increasing concentrations. The standard drug IC_{50} value was observed to be 49.25 µg/ml. Therefore, the nanocomposite showed the significant DPPH scavenging activity.

3.9. Anti-inflammatory activity

3.9.1. Inhibition of albumin denaturation

The synthesized nanocomposite's anti-inflammatory property was tested against the decomposition of bovine serum albumin. The inhibition capacity of a synthesized nanocomposite is shown in Table 2b. The inhibition of albumin denaturation such as 18.32 ± 0.96, 24.15 ± 1.04, 28.03 ± 2.01, 36.13 ± 3.21, 40.23 ± 4.35 µg/ml respectively at different concentrations (20–100 µg/ml) was observed and IC_{50} was observed to be 126.7 µg/ml. Similarly, the radical scavenging activities of sodium diclofenac were performed and the results were between 14.63 ± 1.76 to 92.83 ± 2.02 µg/ml with increasing concentrations. The standard drug IC_{50} value was observed to be 216.6 µg/ml. Therefore, the nanocomposite showed the significant anti-inflammatory activity.

3.10. Toxicity of zebrafish

3.10.1. Anatomy of heart

The control has an intact bulbus arteriosus, atrium, and ventricle (indicated by black arrows). Morphologically the size and shape of the heart appear apposite with thin internal trabeculae, muscu-

Table 1b
Antioxidant ABTS assay was done at different concentration from 20 to 100 µg/mL. The assay was repeated thrice and the results were expressed as mean ± SD.

Samples (Nanocomposite)	Concentrations (µg/ml)					IC_{50} value (µg/ml)
	20	40	60	80	100	
Nanocomposite	± 1.24	± 1.21	± 1.38	± 1.21	± 1.18	
Ascorbic acid (Std)	± 1.32	± 1.35	± 2.26	± 4.56	± 5.55	

Table 2a
Antioxidant DPPH assay was done at different concentration from 20 to 100 µg/mL. The assay was repeated thrice and the mean values were expressed as mean ± SD.

Samples (Nanocomposite)	Concentrations (µg/ml)					IC_{50} value (µg/ml)
	20	40	60	80	100	
Nanocomposite	± 1.29	± 1.18	± 1.18	± 1.22	78.12 ± 1.12	
Ascorbic acid (Std)	± 1.35	± 1.37	± 2.80	± 3.35	± 4.46	

Table 2b
Inhibition of albumin denaturation was carried out at different concentration from 20 to100µg/mL. The assay was repeated thrice and the mean values were expressed as mean ± SD.

Samples (Nanocomposite)	Concentrations (µg/ml)					IC_{50} value (µg/ml)
	20	40	60	80	100	
Nanocomposite	± 1.29	± 1.18	± 1.18	± 1.22	78.12 ± 1.12	
Ascorbic acid (Std)	± 1.35	± 1.37	± 2.80	± 3.35	± 4.46	

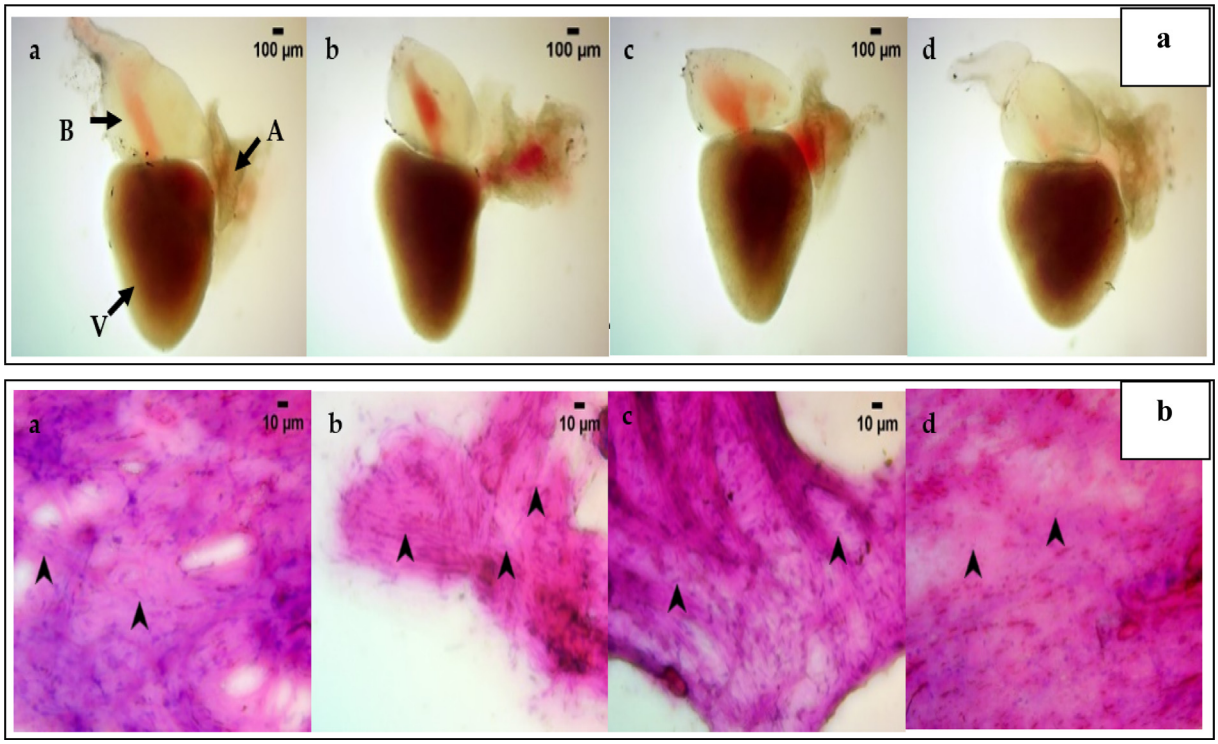

Fig. 3. A&b: 3a- heart anatomy of zebrafish treated with nanocomposite concentration of 1 ng (b), 10 ng(c), and 100 ng (d). Control (a) shows the intact bulbus arteriosus, atrium, and ventricle (indicated by black arrows). The 1 ng (b), 10 ng(c), 100 ng (d) treated dilution groups, shows thin internal trabeculae muscular walled atrium, with size and shape similar to control (a). The image is viewed observed under Labomed LX 400 Light microscope at 40X magnification. 3b. Heart cytology of zebrafish treated with nanocomposite concentration of 1 ng (b), 10 ng(c), 100 ng (d). Control (a) shows the definite cell distribution, with an elongated nucleus and epithelial cells without the presence of inflammatory cells. The 1 ng (b) group shows the darkly stained and shrunken structure identifies cardiomyocyte distribution without cardiomyocyte necrotic cells, which is similar to control (a) group. In 10 ng(c), and 100 ng (d) observed a higher proportion of apposite cardiomyocyte cells without epithelial cells but no necrotic cardiomyocyte cells as compared to control(a). The image was observed under Labomed LX 400 Light microscope at 400X magnification.

lar walled atrium, and dense coloration of the ventricle enriched with blood load. Then studied the control and treated dilution groups for morphological changes. Fig. 3a shows the 1, 10, and 100 ng treated dilution groups, the size and shape of the heart appear apposite with thin internal trabeculae muscular walled atrium. Overall, upon comparison with control, treated dilution groups, namely- 1, 10, and 100 ng, do not exhibit any adverse toxicity confining to the apposite morphology of the heart.

3.10.2. Cytology of heart

Fig. 3b shows the cytology of heart. The Control shows a definite cell distribution, such as cardiomyocytes with an elongated nucleus and epithelial cells without the presence of inflammatory cells. In the 1 ng treated dilution group, the heart cytology exhibits the apposite. The darkly stained and shrunken structure identifies cardiomyocyte distribution without cardiomyocyte necrotic cells. The study observed a higher proportion of apposite cardiomyocyte

cells without epithelial cells in 10 and 100 ng treated dilution groups. Overall, upon comparison with control, the 1, 10, and 100 ng treated dilution groups had no necrotic cardiomyocyte and epithelial cells, which translates to the absence of toxicity in heart cytology.

3.10.3. Anatomy of liver

In the control group, the intact structure of liver with a continuous serosa layer forms the outermost layer of the parenchyma. The central veins run through the longitudinal center of each lobe and the scattered portal vein throughout the parenchyma. Mor-

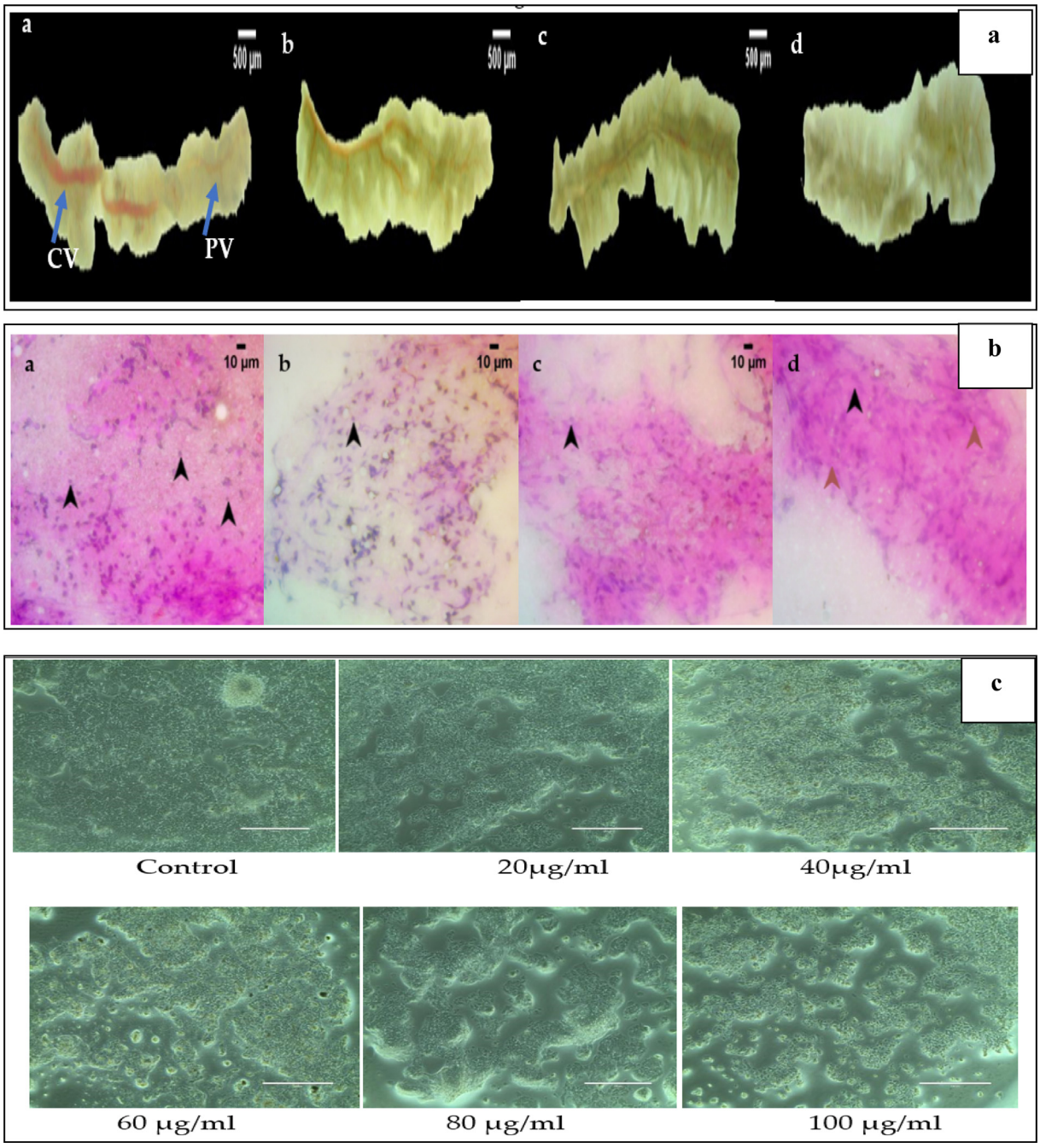

Fig. 4. a&b: 4a- Liver anatomy of zebrafish treated with nanocomposite concentration of 1 ng (b), 10 ng(c), 100 ng (d). Control (a) shows the intact structure of liver with a continuous serosa layer forms the outermost layer of the parenchyma. The central veins run through the longitudinal center of each lobe and the scattered portal vein throughout the parenchyma. The 1 ng (b), and 10 ng(c) treated groups shows the liver anatomy similar to control (a). In 100 ng (d) group the liver appears normal with the entire parenchyma, whereas the central vein appears mildly pale. The anatomical image were viewed under Labomed CM4 stereomicroscope at 10X magnification. 4b-The liver cytology of zebrafish treated with nanocompsite concentration of 1 ng (b), 10 ng(c), 100 ng (d). Control (a) the cytological features with evenly distributed hepatocytes with no evident cellular necrosis. The parenchyma of the liver is composed of hepatocytes with a spherical nucleus on the eosinophilic cytoplasm. In 1 ng (b), and 10 ng(c) group shows the uniform distribution of the stain uptake appeared with well-defined hepatocytes on the eosinophilic cytoplasm, which is similar to control (a) group. In 100 ng, (d) nanocomposite treated group shows the shrunken nucleus identified no necrotic hepatocytes. The cytological image is observed under Labomed LX 400 Light microscope at 400X magnification. c. Effect of different concentration of nanocomposite on cytotoxicity of Hep G2 (Liver cancer) cell line as determined by the MTT assay.

phologically, the liver appears apposite in size, shape, and color. The 1 and 10 ng treated dilution groups seem to have a morphologically apposite central vein enriched with blood supply and intact parenchyma with continuous serosa. At the 100 ng treated dilution group morphologically, the liver appears normal with the entire parenchyma, whereas the central vein appears mildly pale. Overall, upon comparison with control, the 1, 10, and 100 ng treated dilution groups had a morphologically apposite size, shape, and color of liver which shown in Fig. 4a.

3.10.4. Cytology of liver

Control cytology shows the cytological features with evenly distributed hepatocytes with no evident cellular necrosis. The parenchyma of the liver is composed of hepatocytes with a spherical nucleus on the eosinophilic cytoplasm. The 1 ng treated dilution group shows more apposite hepatocytes without necrotic hepatocytes. In the 10 ng treated dilution group, a uniform distribution of the stain uptake appeared with well-defined hepatocytes on the eosinophilic cytoplasm. In 100 ng treated dilution group, the shrunken nucleus identified no necrotic hepatocytes. Overall, upon comparison with control, the 1 and 10 ng treated dilution groups had no necrotic hepatocytes and epithelial cells, which translates to the absence of toxicity in liver cytology (Fig. 4b).

3.10.5. Novel dive tank test

Fig. 6a represents the novel dive tank test with the mean of the control and treated dilution groups, namely 1, 10, and 100 ng. Novel dive tank is a cognitive test that helps to assess the adult zebra fish anxiety-like behavior. The total time spent by the fish in each zone showed a significant difference. Overall, the 100 ng treated dilution group noted mild anxiety compared with the control.

3.10.6. Swim velocity

Fig. 6b represents the swimming velocity of zebra fish. The swimming kinematics, a locomotor assay, helps procure an understanding of the locomotor activity of the fish. The 1, 10, and 100 ng treated dilution group showed a similar swim velocity, which translates no toxicity compared to control.

3.11. In vitro study on Hep G2 cell line

3.11.1. Cytotoxic activity of gelatin-syringic acid/ZnO nanocomposite

The MTT assay results the cytotoxic activity of nanocomposite in liver cancer cells (Hep G2), which are shown in Fig. 4c. The effects of distinct concentrations of nanocomposite (20, 40, 60, 80, and 100) μg/mL are shown on Fig. 6c. The result exhibited that the nanocomposite concentration at 20 μg/mL showed slight decrease in cell viability. As the nanocomposite concentration increased to 40, 60, and 80 μg/mL, a significant reduction in cell viability of 65.4%, 48.2%, 35.6% respectively was observed. At 100 μg/mL a drastic decrease in cell viability has been observed to be 19.2%, thus the cytotoxic effect of nanocomposite is concentration-dependent ($P < 0.05$ each).

3.11.2. Apoptotic detection by AO/PI staining

The apoptosis potential of nanocomposite on Hep G2 cells is shown in Fig. 5a. To recognize both early and late apoptosis nanocomposite treated Hep G2 cells were labeled by Acridine orange/ Propidium Iodide (AO/PI) dual stain and examine under fluorescence microscope. The nanocomposite treated Hep G2 cells displayed remarkable apoptosis-associated changes. The result exhibited an increase in early apoptotic cells with granular green colored nucleus and late apoptotic cells depicted bright orange color with condensed chromatin in nucleus. No major apoptosis was observed in untreated control cells.

3.11.3. Reactive oxygen species

The levels of reactive oxygen species (ROS) were measured by 2′-7′dichlorofluorescin diacetate (DCFH-DA) staining s shown in Fig. 5b. Nanocomposite treated Hep G2 cells were stained with DCFH-DA to detect the ROS production. The result exhibited that the nanocomposite treated Hep G2 cells had an significant ROS production, which has been observed by the appearance of strong DCF-stained green fluorescence in Hep G2 cells whereas the control samples showed faded green fluorescence. Thus the nanocomposite has the ability to induce ROS-mediated cell death.

3.11.4. Mitochondrial membrane potential

Rhodamine staining was used to determine mitochondrial membrane potential (MMP) levels and the image were shown in Fig. 5c. The result exhibited that the uptake of fluorochrome was considerably lower than that of untreated Hep G2 cells. The decreased green fluorescence in nanocomposite treated cells implies the breakdown of the mitochondrial membrane and thus increased mitochondrial dysfunction, which was considered to be an initial and irreversible step of apoptosis.

4. Discussion

Recently, researchers have concentrated on the development of phytochemical-based nanoparticles for therapeutic applications. The hydrothermal method, sol–gel method, and the co-precipitation method are some of the techniques that have been developed to synthesize ZnO nanoparticles (Kołodziejczak-Radzimska and Jesionowski, 2014). In this study, the synthesis of a syringic acid-gelatin-ZnO nanocomposite was performed using the co-precipitation method. The UV spectroscopic result revealed an absorption peak at 280 nm confirming the synthesis of the nanocomposite. Panda et al. (2017) reported similar results, where ZnO nanoparticles synthesized from milky latex of C. gigantea showed a peak at 280 nm. In another study, a peak at 370 nm was observed for chitosan-loaded gelatin polymer composed of ZnO nanoparticles.

The XRD spectral peaks of synthesized nanocomposite revealed five prominent peaks at 32.509, 33.200, 34.56, 40.401, and 59.281, which showed the crystalline nature of ZnO nanoparticle in the synthesisednanocomposite. These results are consistent with the study of Han et al. (2016) wherein the XRD patterns of ZnO NPs had crystallite sizes ranging from 32.5 (100), 33.2(002), and 34.56 (101) nm and was assigned the hexagonal phase. The study further confirmed the purity of synthesized nanocomposite, because it solely included distinctive XRD peaks.

FTIR measurements were used to determine the capping of biomolecules and stabilizing efficient of the nanocomposite. In this study the acute peak around 864 cm^{-1} exhibited the existence of hydroxyl '‾OH' groups. The narrow peak at 3370 cm^{-1} showed the presence of aromatic ring structure. The narrow peaks below 3000 cm^{-1} showed the presence of aliphatic compounds. The rise at 1770 cm^{-1} showed the occurrence of carbonyl compounds (C = C). The strong narrow peak at 1616 cm^{-1} showed the presence of double bond in the synthesized nanocomposite. The zincoxide present in the synthesized nanocomposite shows the absorption peak at 543 cm^{-1}. Synthesis of ZnO nanoparticle with biodegradable polymer (Gum Tragacanth) showed an ZnO absorption peak at 545 cm^{-1}(Kalpana et al., 2014). Analysis of the FTIR spectra of the syringic acid and the synthesized nanocomposite revealed a narrow peak at a frequency of 420 cm^{-1}, which indicates the existence of syringic acid in the synthesized nanocomposite. This data is in reliable with the study of Ning Yang et al., 2020 on ZnO nanoparticle-loaded syringic acid which exhibited the syringic acid extended peak from 3434 cm^{-1} to 444 cm^{-1}. The FTIR spectral

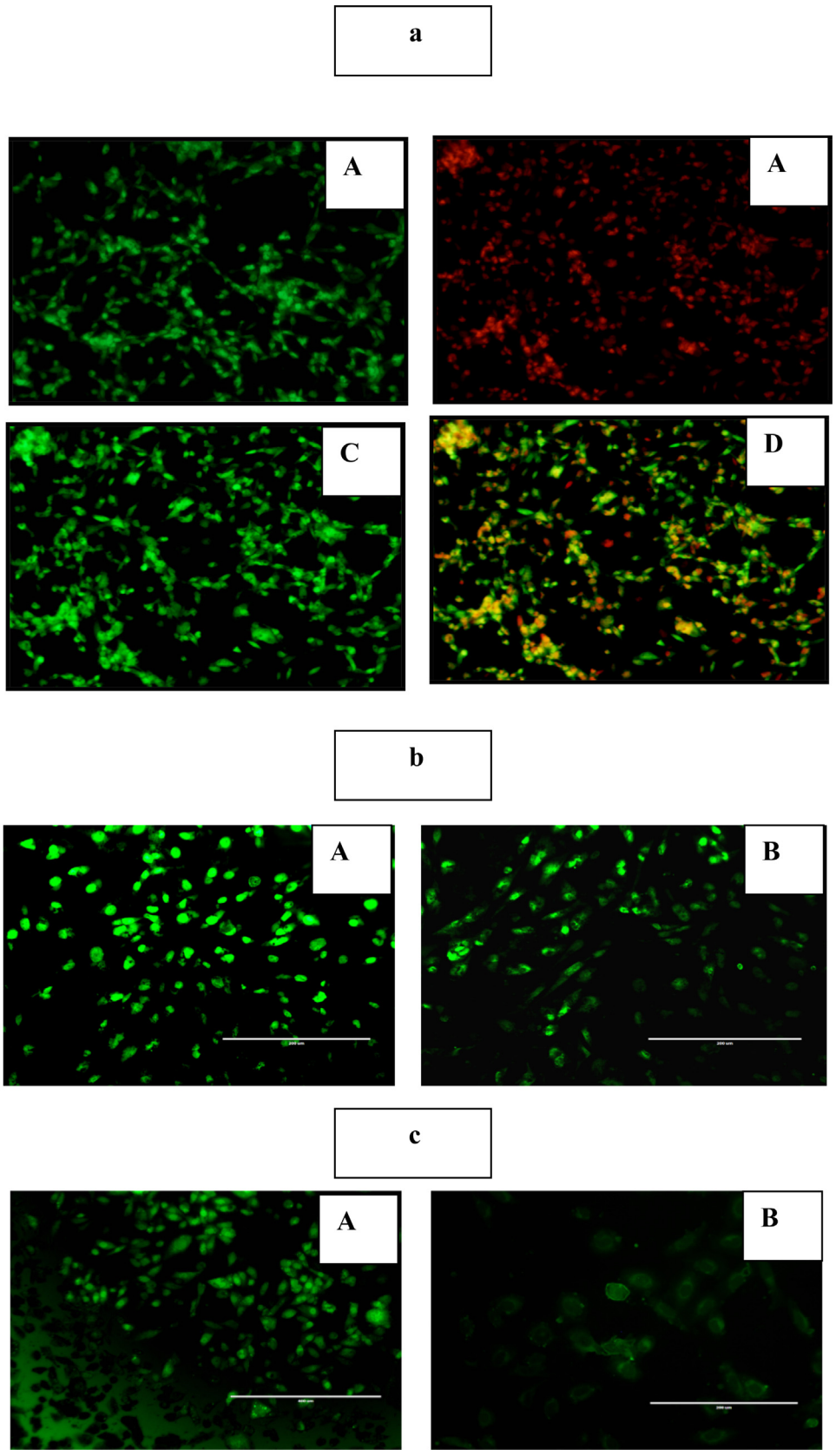

Fig. 5. A-c: 5a-fluorescence microscopy images of hep g2 cell line treated nanocomposite. group (a) control untreated cells shows no major apoptosis. group (b) treated with ao shows the early apoptotic cells with granular green-colored nuclei. group (c) treated with pi shows the late apoptotic cells are bright orange in color and had condensed chromatin in their nuclei. group (d) dual staining for induction of apoptosis. 5b-the nanocomposite induced oxidative stress on apoptotic-associated intrinsic changes in hep g2 cell line. group (a), control untreated cells shows no ros generation with faded green fluorescence. group (b), the nanocomposite treated group stained with dcfh, which showed strong dcf-stained green fluorescence in hep g2 cells. 5c-the effect of nanocomposite onmitochondrial membrane potential (MMP) on Hep G2 cell line. Control (A) Hep G2 cells absorb rhodamine stain and exhibit a dark green fluorescence. Group (B) Hep G2 cells treated with nanocomposite shows significantly less fluorescence resulting in disruption of the mitochondrial membrane and subsequent rise in mitochondrial dysfunction.

peak at 2941 cm^{-1}, represented the presence of gelatin on synthesized nanocomposite.

SEM analysis of the synthesized nanocomposite showed the flaky structure with a size of about 1.11 nm, similarly the study of Dalia et al. (2015) exhibited the agglomerated form of zincoxide nanoparticle, which has been prepared from zinc acetate dehydrate and sodium hydroxide. An EDS analysis revealed a peak of zinc and oxygen, indicating the presence of ZnO nanoparticles. In this study, the extreme peaks at 45.28% and 30.83%, respectively, represent zinc and oxygen and the small peaks showed the presence of trace amounts of carbon and nitrogen. In compatible with the study Devaraj Bharathi et al. (2019) reported the EDS peaks of chitosan-ZnO nanoparticles in which the extreme peak showed the presence of Zn (37.3%) and O (42.6%). The PDI value of 0.4 exhibited the polydisperse nature of the nanocomposite.

Analyses of the drug in vitro release were carried out with the dialysis bag technique. The capacity of an anticancer formulation to maintain stability at physiological pH while releasing its payload at the tumour site is its most desired property (LiuJ et al., 2014). Fig. 2d shows that at 120 min 90% and 60% of raw syringic acid, and syringic acid from nanocomposite are released respectively. The results exhibited that the nanocomposite has a slow and sustained release of syringic acid than a raw syringic acid.

The ABTS assay determines the antioxidant capacity of the synthesized nanocomposite based on the chemical properties of free radicals formed. The oxidized ABTS cation produces a green–blue stable radical cationic chromophore. The antioxidants capacity to scavenge free radicals is due to their potent ability to donate hydrogen (Vignesh et al., 2021). In this study, the free radical scavenging activity of synthesized nanocomposite were determined by ABTS assay. The antioxidant activity of nanocomposite at different concentration were noted on Table 1b, which showed that nanocomposite of 20 μg/ml has a mean value of 20.23 ± 1.24, whereas at 100 μg/ml the mean value is 65.17 ± 1.18, thus the study conclude that the nanocomposite has significant free radical scavenging activity in a dose dependent manner.

The DPPH activity of synthesized nanocomposite has been determined by the slow color change from deep violet in to pale yellow. The antiradical activity of DPPH is primarily determined by its reducing power and the DPPH reaction in which the oxygen atom's electron density is transferred to the odd nitrogen atom electron (Dhaneswar et al., 2013). Table 2a showed the antioxidant effect of nanocomposite at different concentration from 20 to 100 μg/ml, which has a mean value from 21.97 ± 1.29 to 78.12 ± 1.12 respectively. Since the $IC_{50,}$ value of nanocomposite (47.63 μg/ml) is similar to standard ascorbic acid (49.25 μg/ml) the study concludes that the nanocomposite has a significant antioxidant activity.

Albumin denaturation is the breakdown of hydrogen bonds present in the protein, which modifies the molecular structure of protein. Phytochemicals play a key role in inhibiting the albumin denaturation and show a great anti-inflammatory effect (Abhinaya et al., 2019). In this study, the nanocomposite showed the inhibition of albumin denaturation in a dose dependent manner. Table 2b shows the denaturation of protein at different concentration of nanocomposites as 20, 40, 60, 80, and 100 μg/ml and its mean value are 18.32 ± 0.96, 24.15 ± 1.04, 28.03 ± 2.01, 36.13 ± 3.21 and 40.23 ± 4.35 respectively, thus exhibited an excellent anti-inflammatory activity in a dose dependent manner. The existence of aromatic tyrosine rich and aliphatic threonine and lysine residue binding regions of bovine serum albumin (BSA) caused anti-denaturation. Anti-inflammatory effects may be exhibited by compounds that interact with the aliphatic areas near to the lysine residue on BSA (Rungsinee et al., 2015).

The toxicity of a Gelatin-syringic acid/zinc oxide nanocomposite was tested on the zebrafish model at varied drug concentration. In an acute toxicity research, it is essential to assess the behavioural, anatomical, and cytological alterations caused by the synthesized nanocomposite on zebrafish (Diego et al., 2019). To evaluate any negative effects on zebrafish, a logarithmic dosage (LD_{50}) test were conducted. As the results indicated no negative effects, the dosages of 1 ng, 10 ng, and 100 ng of synthesized nanocomposite have been taken into consideration for an acute toxicity study. In zebrafish, the heart is anteroventral and is located in the thoracic cavity between the pectoral girdle and operculum. It has four sections: the atrium, sinus venous, ventricle, and bulbous arteriosus. It begins beating between 22 and 26 hpf, creates a complete set of ion channels, and controls metabolism (Amir et al., 2020). Fig. 3a and 3b shows the anatomy and cytology of the zebrafish heart that treated with the concentration of 1 ng, 10 ng, and 100 ng, which showed no cardio toxic effects as compared with control group. Similarly, Le Gu et al. (2022) investigated the cardiotoxic effects of FoliumArtemisiae argyicarbonisatum methanol extract, which dramatically lowered the heart rate of zebrafish. Furthermore, research has revealed that quercetin has less toxicity on zebrafish (Harishkumar et al., 2019). The liver carries out several vital bodily processes, and changes in this organ may be a sign of harm to the biotransformation, metabolism, and excretion of certain chemicals. As a result, liver anatomy and cytology is an essential biomarker for assessing xenobiotic effects (Guo-Di et al., 2015). Fig. 4a and 4b exhibit the anatomy and cytology of liver at the concentration of 1 ng, 10 ng, and 100 ng nanocomposites treated groups, which exhibited the absence of necrotic cells, and no morphological changes in the liver. In contrast, the study of Kexin Wang et al. (2021) observed the liver toxicity of quercitin and thioacetamide on zebrafish, and proved that quercitin had no toxic effects on liver where as the thioacetamide had little toxic effects on liver. The behavioural changes of zebrafish after exposed to gelatin-syringic acid/zincoxide nanocomposite was determined by novel dive tank test and swim velocity. Fig. 6a shows the anxiety of zebrafish at 1,10,and 100 ng of nanocomposite concentartion,which has been determined by the dive tank test. Fig. 6b shows the survival rate of zebrafish at 1, 10, and 100 ng nanocomposite treated groupss. The 1 ng, and10ng, treated zebrafish groups has no anxiety, whereas the 100 ng treated shows mild anxiety but no mortality of zebrafish were observed during the study, and also observed the excellent swim velocity in all treated groups. Similarly, the study of Shubham Varshney et al. (2022) showed the toxic effect of 6PPD and 6PPD quinone on zebrafish by determining the behavioural changes on swim velocity, and exhibited that the both 6PPD and 6PPD quinone has the concentration dependent locomotion activity on swimming. Earlier studies have noted that swim behavior assays can be utilized for initial screening of muscular or skeletal phenotypes in a moderated throughput before histology (Brooke et al., 2022).

Gelatin-syringic acid/zinc oxide nanocomposite was analyzed for toxicity on Hep G2 cell lines in order to establish its therapeutic potential. The study revealed that the Hep G2 cell line was more cytotoxic as the nanocomposite concentration increased. Fig. 4c shows the cytotoxic effect of nanocomposite at different concentration of 20, 40, 60, 80, and 100 μg/ml,whereas the cellviabilty get decreased as 85.6, 65.4, 48.2, 35.6, and 19.2 percentage(%) respectively on increasing concentration. The nanocomposite exhibited phenotypic changes such as cell rupture into micro fragments, cell contraction, and cell displacement compared to untreated cells, as shown by the microscopic images of Hep G2-treated cells. The results, therefore, revealed that liver cancer cell line-specific nanocomposite anticancer efficacy was significant. Of all the metal nanoparticles, zinc oxide has been found to be the most biocompatible for drug delivery and to be physiologically inert and non-toxic in normal cells. The results shown above were consistent with those of earlier research, in which syringic acid and

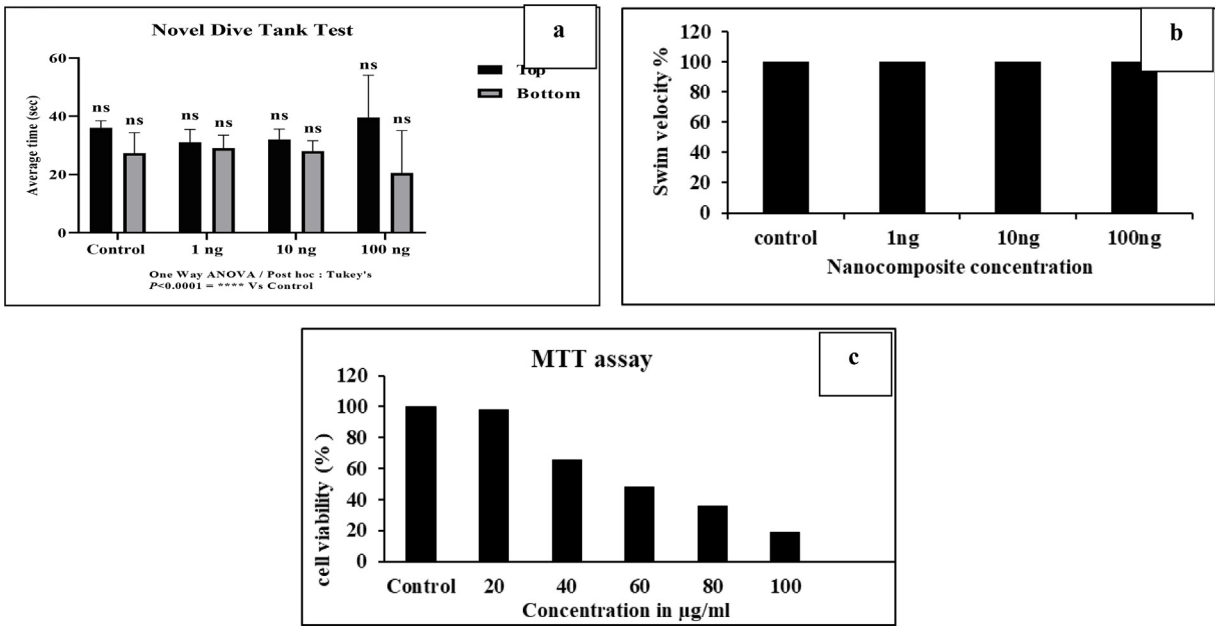

Fig. 6. A-c: 6a-The novel dive tank test with the mean of the control and treated dilution groups, namely 1, 10, and 100 ng. The statistical analysis is calculated by one way-ANOVA, and mean ± SD is $p < 0.0001$as compared with control. 6b-The locomotary activity of zebrafish at different nanocomposite concentration (1, 10, and 100 ng) groups were analyzed by swim velocity. The 1, 10, and 100 ng treated dilution group showed a similar swim velocity, with no toxicity compared to control. 6c-Hep G2 cell viability as measured by the MTT test (data reflects Mean ± SE of three replicates).

biogenic ZnO nanoparticles showed strong cytotoxic effects on the Hep G2 cell line (Kim et al., 2013).

Apoptosis is well established as the primary mechanism of cell death in response to cellular toxicity. Several morphological and physiological alterations, such as chromatin condensation, membrane blebbing, DNA cleavage, and disruption of essential proteins, indicate the highly confined way of cell suicide (Elumalai et al., 2020). The synthesized nanocomposite-treated Hep G2 cells were stained with AO/PI dual stain and viewed under a fluorescence microscope to observe both early and late apoptosis. Fig. 5a shows the apototic effect of nanocomposite on Hep G2 cells, the result exhibited that the untreated (control) cells showed no significant apoptosis and all cells had a consistent green nucleus. Hep G2 cells treated with nanocomposite, however, showed significant apoptosis-related alterations and exhibited a green nucleus and prominent orange spots of contracted chromatin in early apoptotic cells, and post apoptotic cells, respectively. Zahra Sanaeimehr et al. (2018) also found that the zinc oxide nanoparticle synthesized from the extracts of Sargassum muticum algae induces apoptosis in the Hep G2 cancer cell line. When oxidative stress is induced, ROS production increases, and this is earmarked by increased fluorescence intensity as ascertained by the DCFH-DA staining technique and this effect was found to be dose-dependent.

The most prevalent ROS include hydrogen peroxide, hydroxyl radicals, and superoxide radicals. Syringic acid generates ROS naturally by the mechanism of mitochondrial electron transport chain, and under various stimuli that raise ATP demand. Biological variables such as heat exposure as well as some chemicals and carcinogens also induce ROS (Oztekin et al., 2015). They disrupt biological materials like DNA, lipids, and proteins and eventually result in death. Fig. 5b shows the nanocomposite treated HepG2 cell line increasing rate of ROS than control, which exhibits ROS-mediated apoptosis. Evidence suggested that the DCFH-DA substances enter the tumor cells slowly. By cutting the DCFH-DA inside the cancer cells, intracellular esterase's release the non-fluorescent chemical dichlorofluoroscein (DCFH), which is then oxidized by OH groups to produce extremely the luminous molecule, DCF. Thus, it can be concluded that the primary mechanism through which nanocomposite is exported into liver cancer cells is a special cellular absorption process. Previous research suggests that syringic acid induces apoptosis in cancer cells via ROS production. GunjanBisht et al. (2016) reported that ROS are developed by ZnO nanoparticles acting as a redox reaction system, enhancing oxidative stress in cancer cells. It has also been reported that by decreasing the potential of mitochondrial membrane, ZnO nanoparticle generate ROS which induce stress in endoplasmic reticulum thus resulting in the release of caspases (apoptotic protein) and cell death (Dadong et al., 2013). Rhodamine-123, a lipophilic dye, was used to examine the decrease of mitochondrial membrane potential triggered by nanocomposite in Hep G2 cells. Increased ROS production alters the permeability of the mitochondrial membrane, which causes dysfunction in the cells. This dysfunction causes an increase in the liberation of cytochrome *C* enzyme and the onset of apoptosis. Fig. 5c shows the uptake of fluorochrome in nanocomposite treated Hep G2 cells was significantly lower than that of untreated Hep G2 cell line. Similarly, Javed Akhtar et al. (2012) have revealed that mitochondrial membrane rupture mediated by ZnO nanoparticle is significant in apoptosis. These results, therefore, suggest that nanocomposite materials have the ability to trigger apoptosis by depolarizing and sensitizing the potential of the mitochondrial membrane, thus bringing effective cytotoxic action.

5. Conclusion

The study concluded that the gelatin-syringic acid/ZnO nanocomposite exhibited strong antioxidant and anti-inflammatory effects, and found to be non-toxic and highly stable. The synthesized nanocomposite has anticancer potential against Hep G2 cell line, which generates mitochondrial membrane damage by inducing ROS production thereby causing apoptosis. Future clinical investigations on the usage of such therapeutic and metabolically stable nanocomposites might help to explore their anticancer potential in vivo and aid in better prognosis and treatment, thereby improving the quality of patient's life.

Declaration of competing interest

The authors declare that they have no known competing financial interests or personal relationships that could have appeared to influence the work reported in this paper

Acknowledgment

The authors thank the Research Supporting Project for funding this work through Research Supporting Project number (RSPD2023R708), King Saud University, Riyadh, Saudi Arabia.

Appendix A. Supplementary data

Supplementary data to this article can be found online at https://doi.org/10.1016/j.jksus.2023.102909.

References

Abhinaya, S., Padmini, R., 2019. Biofabrication of zinc oxide nanoparticles using pterocarpus marsupium and its biomedical applications. Asian J Pharm Clin Res. 12, 245–249.

Akhtar, M.J., Ahamed, M., Kumar, S., Khan, M.M., Ahmad, J., Alrokayan, S.A., 2012. Zinc oxide nanoparticles selectively induce apoptosis in human cancer cells through reactive oxygen species. Int J Nanomedicine. 7, 845–857.

Bharathi, D., Ranjithkumar, R., Chandarshekar, B., Bhuvaneshwari, V., 2019. Preparation of chitosan coated zinc oxide nanocomposite for enhanced antibacterial and photocatalytic activity: As a bionanocomposite. Int J BiolMacromol. 15 (129), 989–996.

Chanchal, A., Akhtar Husain, S., KamraVerma, A., 2012. In-vitroPhysico-chemical evaluation of Biopolymeric Nanoparticles. Journal of Pharmacy Research 5, 1387–1397.

Dhaneswar, D., Bikash, C., Pinkee, P., Amarjyoti, K., Swapan, Dolui, 2013. Synthesis of ZnO nanoparticles and evaluation of antioxidant and cytotoxic activity. Colloids and Surfaces B: Biointerfaces 111, 556–560.

Elumalai, K., Kithiyon, M., ChinnaRani, I.J., Pannerselvam, B., Thiyagarajan, D., 2020. Syringic acid induces apoptosis in human oral squamous carcinoma cells through mitochondrial pathway.ApplOrganomet. Chem 24, 40–45.

Habiba, A.A., Ahmed, M.A., Faten, A., Salah, H.S., Hanan, F.A., Amr, N., Salama, Z.A., 2021. Nano-formulations of hesperidin and essential oil extracted from sweet orange peel: Chemical Properties and Biological Activities Egypt. Journal of Chemistry 64, 5373–5385.

Han, Z., Yan, Q., Ge, W., Liu, Z.G., Gurunathan, S., De Felici, M., Shen, W., Zhang, X.F., 2016. Cytotoxic effects of ZnO nanoparticles on mouse testicular cells. Int J Nanomedicine. 2016 (11), 5187–5203.

Harishkumar., Rajendran., Reddy., Lakki Pramod Kumar., Karadkar., Shivam H., Murad., Musa Al., Karthik., Saravanan Sibi., Manigandan., Saravanan., Selvaraj., Chinnadurai Immanuel., Christopher., JohnSamuel Godwin., 2019. Toxicity and Selective Biochemical Assessment of Quercetin, Gallic Acid, and Curcumin in Zebrafish. Biological and Pharmaceutical Bulletin, 42(12), 1969–1976. doi:10.1248/bpb.b19-00296.

Hassan, H.F.H., Mansour, A.M., Abo-Youssef, A.M.H., Elsadek, B.E.M., Messiha, B.A.S., 2017. Zinc oxide nanoparticles as a novel anticancer approach; in vitro and in vivo evidence. Clinical and Experimental Pharmacology & Physiology. https://doi.org/10.1111/1440-1681.12681.

Kalpana, H., Sanjay, B., Amit, H., Prakash, H., Kakasaheb, M., Jalinder, A., Nishigandh, P., Vasant, C., 2014. Novel Green Route of Synthesis of ZnO Nanoparticles by Using Natural Biodegradable Polymer and Its Application as a Catalyst for Oxidation of Aldehydes. Journal of Macromolecular Science, Part A: Pure and Applied Chemistry 51, 941–947.

Doaa S. R. Khafaga., Eid,M.M. c., Mohamed Diaa Abd El-Maksoud d., Mie afify d., Mona H. Mohamed e., Abdel Razik H. Farrag f., Rana A. A. Nagy a., Heba K.A., Elhakim a., 2022. Green Synthesis of Zinc oxide Nanocomposite Using Fusarium oxysporum and Evaluation of the Anticancer Effect on Hepatocellular Carcinoma. Egyptian journal of chemistry.Volume 65, Pages 197-207. 10.21608/EJCHEM.2021.91841.4361.

Kim, A.R., Ahmed, F.R., Jung, G.Y., Cho, S.W., Kim, D.I., Um, S.H., 2013. Hepatocyte cytotoxicity evaluation with zinc oxide nanoparticles. Journal of BiomedicalNanotechnol. 9, :926–9.

Kołodziejczak-Radzimska, A., Jesionowski, T., 2014. Zinc Oxide-From Synthesis to Application: A Review. Materials (Basel). 7, 2833–2881.

Le, G.u., Wang, X., Shao, X., Ding, Y., Li, Y., 2022. Study on chemical constituents of Folium Artemisiae argyi Carbonisatum, toxicity evaluation on zebrafish and intestinal hemostasis. Saudi Pharmaceutical Journal 30, 532–543. https://doi.org/10.1016/j.jsps.2022.02.018.

Liu, J., Huang, Y., Kumar, A., Tan, A., Jin, S., Mozhi, A., 2014. pH-sensitive nano-systems for drug delivery in cancer therapy. Biotechnol Adv. https://doi.org/10.1016/j.biotechadv.2013.11.009, PMID 24309541.

Mahesh, P.M., Sagar, R.P., Chandrakantsing, V.P., Gaurav, A.S., Mahesh, N.S., Prashant, K.D., Jitendra, B.N., Abhijeet, D.K., 2021. Recent advances in phytochemical-based Nano-formulation for drug-resistant Cancer. Medicine in drug discovery.

Majumdar, D., Jung, K.H., Zhang, H., Nannapaneni, S., Wang, X., Amin, A.R., Chen, Z., Chen, Z.G., Shin, D.M., 2014. Luteolin nanoparticle in chemoprevention: in vitro and in vivo anticancer activity. CancerPrev Res (Phila). 7, 65–73.

Mishra, P.K., Mishra, H., Ekielski, A., Talegaonkar, S., Vaidya, B., 2017. Zinc oxide nanoparticles: a promising nanomaterial for biomedical applications. Drug Discov Today. 22, 1825–1834.

Mohanty, C., Das, M., Sahoo, S.K., 2012. Emerging role of nanocarriers to increase the solubility and bioavailability of curcumin. Expert Opin Drug Deliv. 11, 1347–1364.

Panda, K.K., Golari, D., Venugopal, A., Achary, V.M.M., Phaomei, G., Parinandi, N.L., Sahu, H.K., Panda, B.B., 2017. Green Synthesized Zinc Oxide (ZnO) Nanoparticles Induce Oxidative Stress and DNA Damage in Lathyrus sativus L. Root Bioassay System. Antioxidants (Basel) 6, 35.

Rungsinee, P., Wantida, C., Songyot, A., 2015. Curcumin-loaded multi-valent ligands conjugated-nanoparticles for antiinflammatory activity. Int J Pharm PharmSci 7, 203–208.

Srinivasulu, C., Ramgopal, M., Ramanjaneyulu, G., Anuradha, C.M., Suresh Kumar, C., 2018. Syringic acid (SA) - A Review of Its Occurrence, Biosynthesis, Pharmacological and Industrial Importance. Biomed Pharmacother. 108, 547–557.

Shubham Varshney., Adnan H., Gora., Prabhugouda Siriyappagouder., Viswanath Kiron., Pål A., 2022. Olsvik. Toxicological effects of 6PPD and 6PPD quinone in zebrafish larvae. Journal of Hazardous Materials 424 127623 https://doi.org/10.1016/j.jhazmat.2021.127623.

Vignesh, A., Selvakumar, S., Vasanth, K., 2021. Green synthesis and characterization of zinc oxide nanoparticles using BerberistinctoriaLesch. leaves and fruits extract of multi-biological applications.Asian J Pharm. Clin Res. 6, 128–147.

Wang, K., Deng, Y., Zhang, J., Cheng, B.o., Huang, Y., Meng, Y., Zhong, K., Xiong, G., Guo, J., Liu, Y.i., Huiqiang, L.u., 2021. Toxicity of thioacetamide and protective effects of quercetin in zebrafish (Danio rerio) larvae. Environmental Toxicology. https://doi.org/10.1002/tox.23323.

Watkins, R., Wu, L., Zhang, C., Davis, R., Xu, B., 2015. Natural product-based nanomedicine: recent advances and issues. International JournalNanomedicin. 10, 6055–6074.

Yang, N., Qiu, F., Zhu, F., Qi, L., 2020. Therapeutic Potential of Zinc Oxide-Loaded Syringic Acid Against in vitro and in vivo Model of Lung Cancer. Int J Nanomedicine. 27 (15), 8249–8260.